

UNIVERSITY OF TWENTE.

Faculty of Electrical Engineering,
Mathematics & Computer Science



Trans-Spinal Direct Current Stimulation in Incomplete Spinal Cord Injury Subjects: Analysis of Motor Unit Activity for a New Class of Biomarkers

Antonio de Jesus Gogiascoechea Hernandez

M.Sc. Thesis

January 2019

Supervising committee:

Dr.ir. Sartori

Dr. Yavuz

Dr.ir Buitenweg

Faculty of Electrical Engineering,
Mathematics and Computer Science
University of Twente
P.O. Box 217
7500 AE Enschede
The Netherlands

Trans-Spinal Direct Current Stimulation in Incomplete Spinal Cord Injury Subjects: Analysis of Motor Unit Activity for a New Class of Biomarkers

Antonio Gogeochea

Abstract—Electrophysiological changes after trans-spinal direct current stimulation (tsDCS) in incomplete spinal cord injury (SCI) subjects are not well understood. Presumably, cathodal tsDCS facilitates motor function after stimulation is administered in healthy subjects. The aim of this study is to investigate motor unit (MU) features that help describe the effects of tsDCS on incomplete SCI subjects. Based on the data of the double-blind, sham-controlled crossover study of Kuck et al. [1], neural activity of the soleus muscle from one chronic, incomplete SCI subject was analyzed in time and frequency domain. The protocol recorded high density-electromyography (HD-EMG) during plantar flexion sub-maximal contractions before and just after cathodal and sham tsDCS (2.5 mA, 15 min). In frequency domain, several features were obtained from the coherence between two cumulative spike trains (CSTs), which were generated from sets of single motor units (MUs). The coherence peaks and areas of the delta band (0-5 Hz) showed a decrease after cathodal tsDCS and no effect after sham tsDCS. This suggests that cathodal tsDCS decreases the strength of the common drive, which is likely due to an enhanced afferent feedback as secondary common synaptic input. Supporting this hypothesis, it was also found that the number of MUs in the CSTs reaching a plateau in coherence was greater after cathodal tsDCS. In time domain, a decrease in the cross-correlation peaks between smoothed CSTs confirmed the decrease in strength of the common drive found in frequency domain. Moreover, the coefficient of variation of the smoothed CSTs indicated a possible increase in steadiness (decrease in fluctuations) after cathodal tsDCS and no change after sham tsDCS. However, the coefficient of variation of the first common component (FCC, first principal component) as well as the average discharge rate did not reveal any change. The present study provides a novel MU-based analysis of the effects of cathodal tsDCS on lower limb motor impairment due to incomplete SCI. At a later stage, these findings may lead to robust biomarkers for a closed-loop modulation of the corticospinal excitability.

I. INTRODUCTION

Spinal cord injury (SCI) refers to a damage to any part of the spinal cord that usually results in loss of motor and sensory function below the site of the injury [2]. It is often caused by physical trauma to the vertebrae, ligaments or disks of the spinal column in consequence of accidents, falls, sports injuries, etc. Incomplete SCI is the most common type of SCI [3] and occurs when the injury is not severe enough to entirely interfere with the spinal function. Typically, people who suffer incomplete SCI experience a decreased voluntary control of limbs, spasticity, paresis spasms, and pain, among other symptoms. Yet, they are more likely to experience improvements after long-term rehabilitation.

Currently, very few countries across the world report epidemiological data on the prevalence (actual amount of existing cases) and the incidence (amount of new cases

within a period of time) of SCI. According to an up-to-date extended review conducted by Singh et al. [4], the countries with the highest prevalence of SCI are United States of America (906 per million), Australia (681 per million), and Iceland (526 per million). The regions with the lowest SCI prevalence include the Rhone-Alpes region, France (250 per million) and Helsinki, Finland (280 per million). With regards to the Netherlands, there is no reliable approximation of the SCI prevalence to date. However, a recent study conducted by Nijendijk JH et al. [5], estimates that the incidence of SCI was 14 per million per annum in 2010. Other studies indicate higher rates of annual incidences in New Zealand (49.1 per million), United States of America (40.1 per million), Estonia, and Japan. Figure 1 shows the number of incidence of SCI across the world according to Singh et al. [4].

After incomplete SCI, plastic changes of neural circuits manifest in several levels of the central nervous system [6, 7]. Whereas the corticospinal tract remains intact above the injury, cortical inputs to spinal segments (Appendix A) below the injury are reduced due to disruption and demyelination of axons at the injury level [8]. This reduction affects directly the motor, sensory and inter-neurons below the injury. As a motor unit (MU) reflects the amplified activity of a single alpha-motor neuron, it provides neuronal level information about neuromuscular control at spinal cord. Thus, it is fundamental concept for analyzing abnormalities in neuromotor function due to SCI. A MU consists of an alpha-motor neuron and the skeletal muscle fibers that it innervates. Its behavior can be decomposed from high density-electromyography (HD-EMG, non-invasive technique) recordings through Convolution Kernel Compensation (CKC) algorithms. During sustained voluntary contractions, motor neurons receive common and independent synaptic inputs [9–11]. Classic methods of neuromotor analysis focused on independent inputs or common inputs to few MUs (usually only a pair), mainly because the decomposition was performed manually by visual inspection to identify action potentials [12, 13]. These methods were time-consuming and required high expertise. Nowadays, current automatic decomposition methods allow to analyze common inputs to several concurrently active MUs [14]. As it is proven that the independent inputs are canceled out by the motor neuron pool (a collection of all MUs of a single skeletal muscle) and only the common input approximates accurately to the actual neural drive to muscle [14] (neural signal for force control), it is highly relevant to measure the strength of the common synaptic input. This is typically done by computing the coherence between two

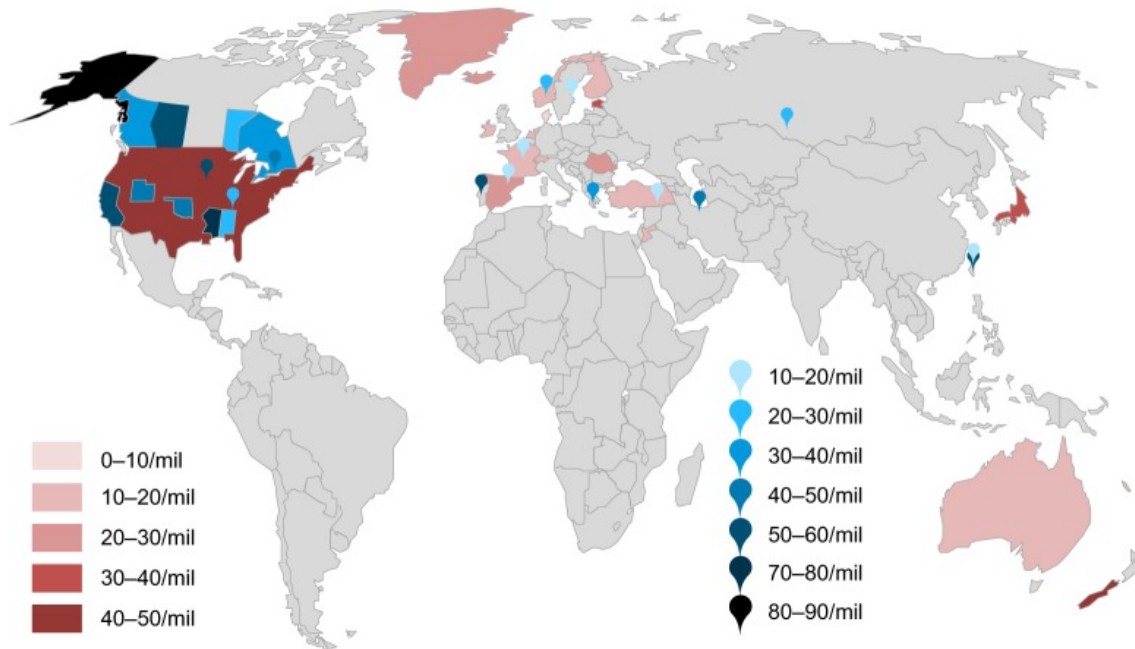


Fig. 1. Relative annual incidences of countries (in red), states/provinces, and regions (in blue). Adapted from Singh et al. [4]

cumulative spike trains (CSTs). The coherence is a measure of linear correlation in frequency domain and allows to assess the degree of *similarity* at different bandwidths. Because the very low frequencies of common synaptic inputs are associated with force generation (common drive) [10, 15], the present study focuses on the delta band (< 5 Hz).

Over the past decade, growing interest has focused on trans-spinal direct current stimulation (tsDCS) due to its non-invasive nature and its ease of application. This type of neurostimulation only involves a pair of sponge electrodes on the skin, delivering a constant direct current (1.5-2.5 mA) to a target region of the spinal cord [16]. Current research on tsDCS relies on classic techniques that use external stimuli to test (indirectly) the excitability of motor neuron pools (H-reflex, F-wave) as well as the overall excitability of the corticospinal tract (motor evoked potentials [MEPs]). On this account, previous studies in healthy subjects suggest a facilitation of cortically elicited muscle actions after cathodal tsDCS [16–19] and a hypothetical inhibitory effect after anodal tsDCS [16, 20, 21]. Due to these promising findings, tsDCS may have also relevant implications for the rehabilitation of SCI; however, its exact underlying mechanisms of action are not yet fully understood. Additionally, these classic techniques present some flaws. For instance, the H-reflex is also affected by other mechanisms such as post-activation (homosynaptic) depression and changes in axonal excitability [22, 23]. Moreover, Hulborn and Nielsen [23] demonstrated that F-waves are relatively insensitive to motor neuron excitability. On the other hand, MEPs may offer a very well-founded measure of corticospinal excitability as they are elicited in peripheral muscles by transcranial magnetic stimulation (TMS) over the motor cortex (multiple impulses

descending in the corticospinal tract). However, their interpretation is limited as the cortical and the spinal excitability cannot be measured in isolation [22]. Therefore, a more specific and straightforward analysis of electrophysiological changes after tsDCS is needed. Whereas the aforementioned studies are based on features that depend on externally elicited stimuli (H-reflex, F-wave and MEPs), the present study offers a direct analysis at the MU level with features that only depend on muscle contraction measurements and MU decomposition.

Based on the CKC decomposition of the double-blind, sham-controlled crossover study of Kuck et al. [1], this research is conducted on repeated measurements of the soleus muscle during isometric contractions from incomplete SCI patients. Following novel methods to describe neuromotor function [9, 14, 24–26], the present study examines the strength and the fluctuations of the common drive in time and frequency domain.

This thesis proposes novel strategies to help distinguish electrophysiological signs of changes in motor neural activity after cathodal tsDCS in incomplete SCI subjects. The results of this thesis may lead to a better understanding of the effects of cathodal tsDCS on lower limb motor impairment after SCI as well as to a closed-loop modulation of the corticospinal excitability at a later stage.

II. METHODS

A. Study protocol

Subjects: The protocol of Kuck et al. [1] was designed for 10 subjects with chronic incomplete SCI but only 4 were finally recruited. The inclusion criteria were as follows: (i) age > 18 years; (ii) good vision (on 2 m distance); (iii)

chronic stage (time since SCI > 12 months); (iv) clear walking impairment but able to walk independently with support (Walking Index for Spinal Cord Injury [WISCI] > 1 and Spinal Cord Independence Measure [SCIM] > 30); (v) motor incomplete SCI (American Spinal Injury Association [ASIA] Impairment Scale C or D); (vi) a stable medical condition; and (vii) injury situated superior to the 9th vertebra. Exclusion criteria were as follows: (i) history of skin diseases that could result in irritation of the skin underneath the electrodes; (ii) history of epilepsy or a known case of epilepsy in a first degree relative; (iii) metallic implants in the body, unrelated to the SCI, in proximity to the stimulation electrodes; (iv) metallic implants in the body, related to the SCI below vertebrae T6; (v) presence of cardiac pacemakers, cochlear implants or implanted brain electrodes; (vi) use of any illegal drugs in the last year; (vii) (possibility of) pregnancy; (viii) current orthopedic problems; (ix) other neurological disorders; (x) chronic joint pain; (xi) history of cardiac conditions that interfere with physical load; (xii) history of severe depression; and (xiii) stable use of anti-spasticity medication.

Experimental procedures: The protocol of Kuck et al. [1] was designed as a double-blind, sham-controlled crossover study. The experimental set-up was divided into three stages: pre-, just after and post-stimulation. For each stage, the subjects were seated on a force-chair which was assembled for isometric ankle plantar-flexion. During the pre-stimulation phase, the maximum voluntary contractions (MVCs) on gastrocnemius and soleus muscles were measured. Subsequently, the subjects performed sub-maximal plantar flexion contractions (at 8%, 15% and 20% MVC) following 9 force tasks in random order. Each sub-maximal voluntary contraction level was performed three times per trial (Figure 2, top figure). A single task consisted of a ramp up (2.5% MVCs), hold (25 s) and ramp down (2.5% MVCs) (Figure 2, bottom figure).

Afterwards, the subjects underwent two types of stimulation in randomized order: cathodal (2.5 mA) and sham tsDCS (ramp up to 2.5 mA and turned off after a few seconds). The configuration was the same for both: the cathode was centered between the 11th and the 12th thoracic vertebrae (~ L3-L5 segments of the spinal cord, Figure 13) and the anode was located on the right shoulder [1, 16]. Stimulation was administered using a custom-build TMSi stimulator (TMS International B.V., Oldenzaal, The Netherlands) while the subjects performed a force tracking task for a period of 15 minutes (8 minutes of force tracking with 3.5 minutes of rest before and after). The task consisted of a mixture of sinusoids with a maximum of 10% MVC.

Lastly, the sub-maximal plantar flexion tasks were repeated immediately after (t0) and 30 minutes after (t30) stimulation. The HD-EMG was recorded using a TMSi Refa multi-channel amplifier (TMS International B.V., Oldenzaal, The Netherlands) with a sampling frequency of 2,048 Hz. 64-channel grid electrodes were placed on the gastrocnemius and soleus muscles during pre-stimulation, t0 and t30. The recordings were offline decomposed into MU spike trains

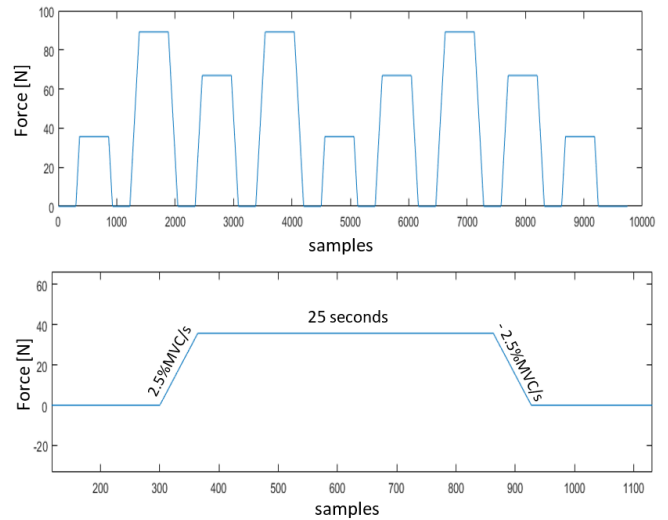


Fig. 2. Top figure: Example of a trajectory with sub-maximal contractions at 8%, 15% and 20% of MVC (each level is measured three times). Bottom figure: close-up of the first ramp. Adapted from Kuck et al. [1]

using CKC algorithms [27].

Limitations: For this exploratory study, only the first subject was considered since the other subjects presented either poor HD-EMG data quality (too few units decomposed, less than 6 in average) or a change in the protocol (half of the stimulation intensity). Moreover, only pre-stimulation and t0 conditions were contemplated as the t30 condition presented multiple missing cases and did not show any consistent behavior. Regarding the muscles, only the results of the soleus muscle are included as the gastrocnemius did not show any consistent trend during earlier stages of the project.

B. Data Analysis

The data were offline analyzed with Matlab R2017b (The Mathworks Inc., Natick, MA, USA). Cumulative spike trains (CSTs) were defined as the sum of individual MU spike trains. Each MU spike train consists of a vector where the value of 1 indicates when a discharge is identified at a time instant and 0 when no discharge is detected (sampling frequency: 2,048 Hz).

A quality control algorithm and three different approaches were conducted: coherence of non-intersecting CSTs (subsection II-D), average of coherence peaks of all possible CST pairs (subsection II-E), and average discharge rate (subsection II-E). The details of the signal processing for the quality criteria and for each approach are described in the following sections.

C. Quality Criteria

As CKC decomposition is a probabilistic iterative procedure to blindly estimate individual spike trains in presence of external noise, errors in the decomposition are inherently expected. Hence, each spike train was inspected for quality control. For this purpose, four quality indices were evaluated: pauses, coefficient of variation (CoV) of the interspike intervals (ISI), silhouette (SIL), and pulse-to-noise ratio (PNR).

TABLE I

COMPARISON BETWEEN QUALITY INDICES FROM LITERATURE AND THIS STUDY. THE THRESHOLDS OF THIS RESEARCH THAT DIFFER TO THE ONES FOUND IN OTHER STUDIES ARE HIGHLIGHTED IN BOLD.

Authors	No pauses	CoV _{ISI}	PNR	SIL
Dideriksen et al. [24]	Visual	-	-	-
Negro et al.[30]	-	-	-	>0.9
Martinez et al.[28]	-	-	-	-
Holobar et al. [27]	Visual	< 0.3	>30dB	-
Laine et al. [25]	<0.5s	-	-	-
This research	<1s	<0.3	>20dB	>0.9

The coefficient of variation of the ISI was calculated as the ratio between the standard deviation of the ISI and its mean value [25, 27, 28]. Only discharges with ISI > 33.3 ms (30 Hz) and ISI < 300 ms (3.3 Hz) were included for the CoV_{ISI} because intervals outside this range may not be physiological for the soleus muscle, and are more likely to be errors from the CKC decomposition [28, 29]. The SIL was obtained from the CKC algorithm. To calculate this measure, the within-cluster point-to-centroid distances are summed, as well as the distances between clusters. The SIL is defined as the difference between these two sums, normalized dividing by the maximum of the two values [28, 30]. Finally, the PNR is the logarithmic ratio (dB) between the means of the innervation pulse train at all time moments in which a MU is estimated to have discharged ($E(\hat{i}^2(n)|_{\hat{i}^2(n) \geq r})$) and not to have discharged ($E(\hat{i}^2(n)|_{\hat{i}^2(n) < r})$) [31]:

$$PNR(\hat{i}(n)) = 10 \cdot \log \left(\frac{E(\hat{i}^2(n)|_{\hat{i}^2(n) \geq r})}{E(\hat{i}^2(n)|_{\hat{i}^2(n) < r})} \right), \quad (1)$$

where $\hat{i}(n)$ denotes the innervation pulse train as a function of samples and r the threshold to detect a pulse.

Table I shows the thresholds found in literature for each index and the thresholds proposed in this study. Since the PNR depends on the quality of the decomposition, its threshold was decreased after visual inspection. Similarly, the threshold of the pauses was increased to compensate for errors in the decomposition or for abnormalities due to SCI.

Based on the aforementioned indices, a quality control algorithm was developed. First, as the subjects performed 25-second sustained sub-maximal contractions, only MUs with no pauses greater than 1s were selected. Additionally, it was checked that at least two of the following conditions were satisfied: CoV_{ISI} < 0.3, PNR > 20dB, SIL > 0.9. These thresholds were fixed for all the ramps in both conditions. Algorithm 1 shows how the quality selection was computed and Figure 3 depicts an example of how it works.

Because the amount of MUs per CST influences the strength of the common synaptic input, motor neuron pools with less than 6 MUs [24] were disregarded as an additional quality requirement.

In order to validate the proposed quality algorithm, the force signal and the smoothed CST (neural drive to the muscle) were compared. If the degree of correlation between signals remained approximately the same after quality con-

Algorithm 1 Quality control

```

for all  $MUs$  do
  if  $pauses < 1s$  then
    if  $\{(CoV_{ISI} < 0.3 \text{ and } PNR > 30dB) \text{ or}$ 
       $(CoV_{ISI} < 0.3 \text{ and } SIL > 0.9) \text{ or}$ 
       $(PNR > 30dB \text{ and } SIL > 0.9)\}$  then
      store  $MU$ 
    else
      remove  $MU$ 
    end if
  else
    remove  $MU$ 
  end if
end for

```

trol, no relevant neural information was lost. Figure 4 shows how the smoothed CST still reflects the behavior of the actual force after some MUs with poor quality were removed.

D. Coherence between non-intersecting CSTs

In this approach, each motor neuron pool was divided into 2 and 3 non-intersecting groups of CSTs. For instance, if the pool contained 6 MUs, 2 CSTs consisting of three units (MU1-MU3 and MU4-MU6) were obtained. Likewise, three groups with non-intersecting units were extracted (MU1-MU2, MU3-MU4 and MU5-MU6). Splitting the motor neuron pool into 2 or 3 groups is a trade-off between having results with more coherence (2 groups) and extracting more data per ramp (3 groups).

In order to estimate the strength of the common drive (delta band), the magnitude-squared coherence was performed between pairs of detrended CSTs using the Welch's periodogram with Hann windows of 1 second, 50% overlap. Only the steady state interval of both smoothed CSTs was considered. Moreover, the coherence values were transformed into standard Z-scores [32] as follows:

$$COH_{Zscore} = \frac{\text{arctanh} \sqrt{COH}}{\sqrt{1/(2N)}}, \quad (2)$$

where N is the number of segments used to calculate the coherence (COH). This conversion accounts for any difference in the number of units in each CST [25]. From these transformed coherence values, significant peaks and areas were extracted in the delta band (0-5 Hz). The significance level was set to 0.05. Figure 5 illustrates an example of two coherence functions during pre- and just after stimulation trials.

E. Average of coherence peaks of all possible CST pairs

Several coherence values were extracted with all possible combinations of CSTs within a motor neuron pool (including CSTs with intersecting MUs) ranging from groups of 1 single unit to $N - 1$ units in each CST. From the aforementioned example of a pool with 6 MUs, this approach also takes combinations into account like: MU1, MU2 & MU1, MU3. As spike trains with several MUs provide a very high number

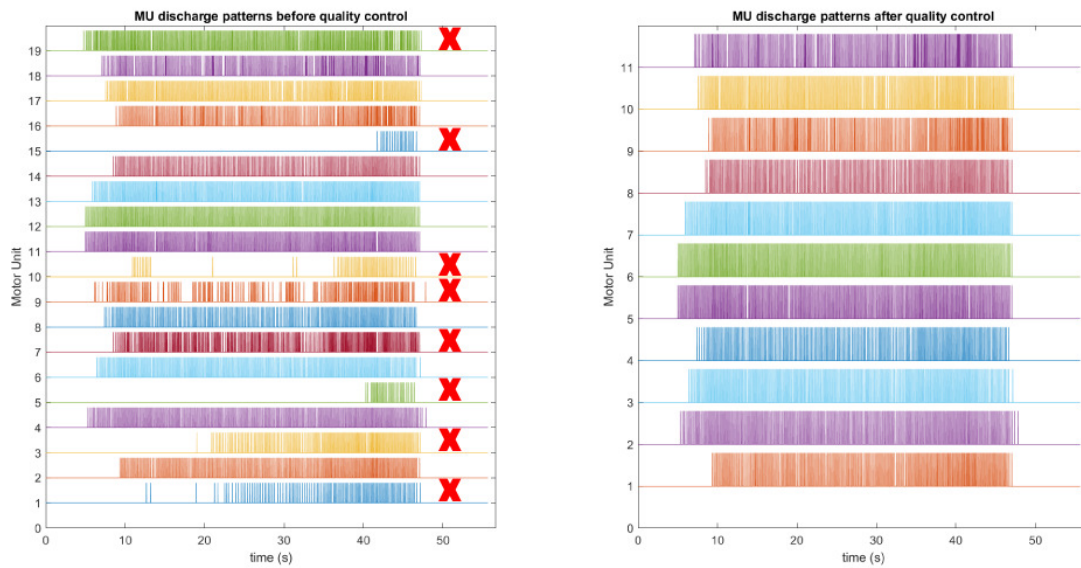


Fig. 3. Example of a motor neuron pool before (left) and after (right) quality control. The red crosses on the left figure indicate the MUs that do not meet the quality criteria and, thus, they are removed after quality control (right).

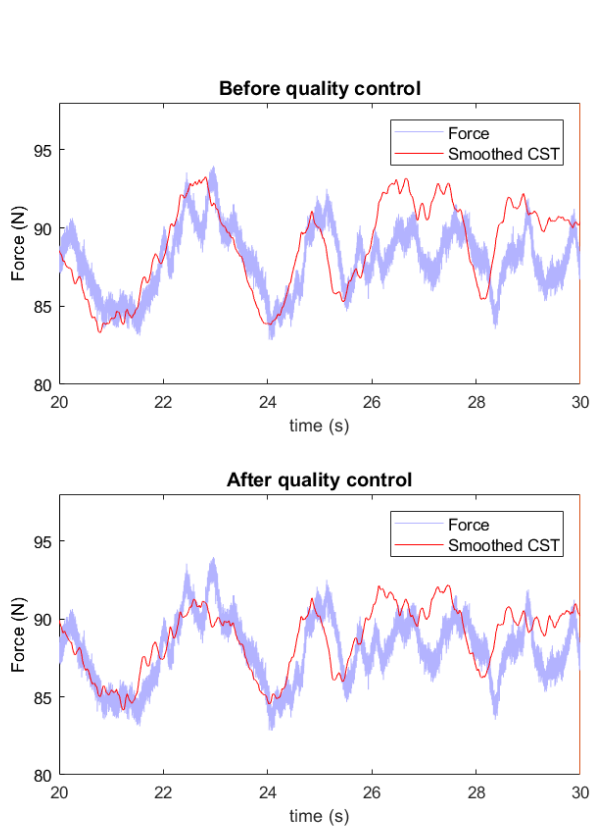


Fig. 4. Comparison between actual force (blue line) and the smoothed CST (red line) before (top) and after (bottom) quality control. Although some spike trains were removed after quality control, the strong correlation between force and smoothed CST remains approximately the same.

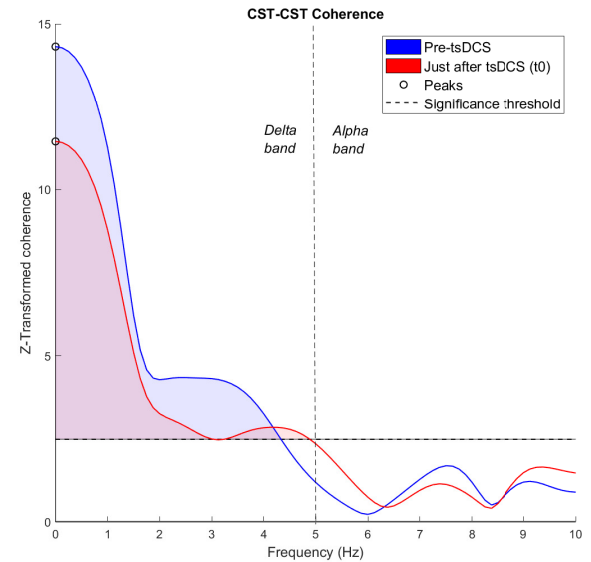


Fig. 5. Z-transformed coherence values between CSTs. The blue and red lines indicate the coherence curves of pre and just after stimulation, respectively. Likewise, their significant areas are colored in light blue and light red. The significant peaks for each curve are indicated with black circles and the black dash line indicates the confidence limit for coherence (0.05).

of possible combinations, the maximum sample size of CSTs was set to 200. The different combinations were chosen randomly with a fixed seed for repeatability.

The coherence was computed the same way as in the previous section. However, due to the hyperbolic shape of the Z-transformation, the values were not converted into Z-scores. The average of the coherence peaks was calculated

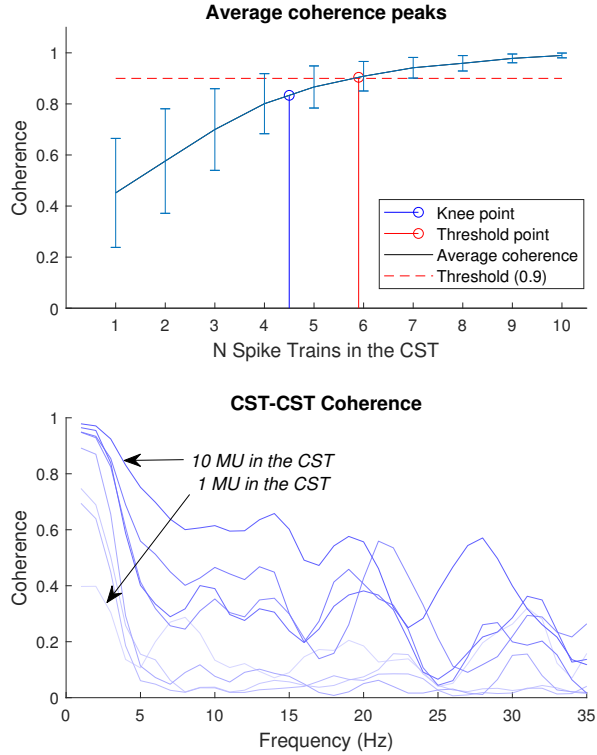


Fig. 6. Top figure: Average of coherence peaks (black curves) between two CSTs as a function of the number of MUs in each CST. The error bars indicate the standard deviation and the vertical blue lines with a circle marker indicate knee points of the curves. The vertical red lines with a circle marker show the amount of MUs required to reach a coherence threshold of 0.9 (dashed red lines). Bottom figure: Examples of the coherence between two CSTs consisting of different numbers of MUs in the CSTs. The lightest blue line corresponds to the coherence of CSTs with 1 MU and the contrast increases with more MUs per CST until $N - 1$ MUs per CST (darkest blue line).

as a function of the group size (N number of units in the CSTs) as shown in Figure 6. The knee point of the curve was obtained as well as the point in which the average of coherence peaks reached a threshold of 0.9. Furthermore, the x -axis (number of units per CSTs) was up-sampled (by a factor of 10) to distinguish between slight differences. The number of MUs required to reach a plateau in coherence (estimated by the knee point or certain threshold) provides also an estimate of the strength of the strength.

F. Time domain approaches

The first dependent variable of the time domain approach was the average discharge rate of the motor neuron pool. As mentioned before in the quality criteria, discharges separated from the following by <33.3 ms and >300 ms (30 and 3.33 pulses per second (pps), respectively) were excluded.

In order to perform a principal component analysis (PCA), the instantaneous discharge rate (IDR) for each MU was computed. The difference between the IDR and the discharge rate is that the former keeps the same sampling points through interpolation. This allows further processing which

was not necessary for the first variable (as it is only an average). As proposed in previous studies [26, 33], the IDR was smoothed with a 400 ms Hann window and detrended with a zero-phase high-pass filter (cut-off frequency of 0.75 Hz). The PCA was performed on the same steady state interval for all MUs using eigenvalue decomposition of the covariance matrix [26]. Figure 7 displays an example of the principal components computation.

The second dependent variable to explore was the coefficient of variation of the first common component (FCC). As the FCC was computed using the detrended IDR (mean value ≈ 0), the coefficient of variation was calculated as the standard deviation of the FCC divided by the sum of the mean discharge rate and the mean FCC. By doing this, the variability of the FCC around the average discharge rate was calculated. Because the FCC accounts for the greatest possible variance of the entire motor neuron pool, its coefficient of variation can be used as an estimate of changes in the steadiness to the neural drive.

To corroborate the estimate of the steadiness, the coefficient of variation of the smoothed CST was computed. A second-order zero-phase Butterworth low-pass filter was used to smooth the CST. A low cut-off frequency (2 Hz) was set to analyze only the common drive.

Similar to the coherence between non-intersecting CSTs (subsection II-D), each motor neuron pool was divided into 2 and 3 smoothed CSTs. Each smoothed CST was detrended by subtracting its mean. The cross-correlation peaks between smoothed CSTs were converted into Z-scores ($CORR_{Zscore} = \text{arctanh} \sqrt{CORR}$). This last variable was used to confirm the results of the coherence analysis.

G. Statistical analysis

The statistical tests were run in IBM SPSS Statistics v.24 (IBM Corporation, New York, USA). The Shapiro-Wilk test was used to check normality, if violated, the corresponding variable was transformed with a logarithmic function. The significance level was set to 0.05.

Student's paired t-tests were performed to check whether there was a significant difference between the time conditions within each experiment (cathodal and sham). Particularly, it was tested if there was a significant change after administering cathodal tDCS, and if there was no significant change after sham tDCS (placebo).

III. RESULTS

Table II shows the statistics, degrees of freedom, and p -values of all variables and tests reported in this study. Further details of the results (mean, standard deviation, standard error of the mean and rates of consistency) can be found in the appendix C (Table III).

Regarding the normality tests (Shapiro-Wilk), only the knee points variable deviated from a normal distribution ($P < 0.05$), hence hereinafter, its logarithmic transformation was used for the following statistical tests.

Figure 8 shows the results for the first approach: coherence peaks and areas of 2 and 3 groups of CSTs per motor neuron

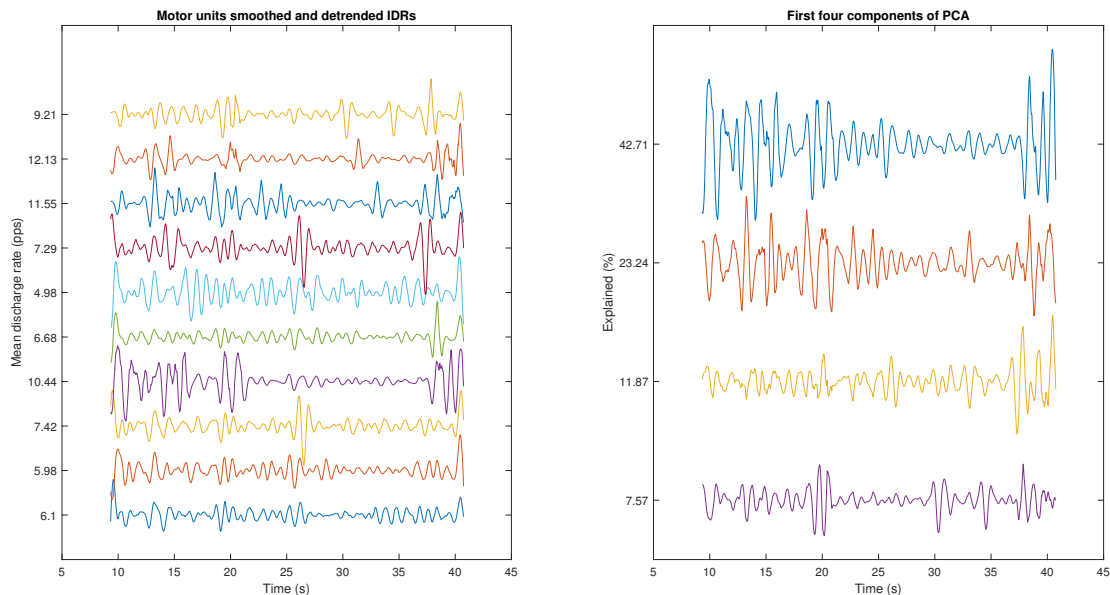


Fig. 7. Left figure: Smoothed and detrended instantaneous discharge rates, each line represents a MU. The y-axis indicates the mean discharge rate per MU. Right figure: their first four principal components. The y-axis indicates the percentage of the total variance explained by each principal component.

pool. As expected, the Student's paired t-test revealed a significant decrease after cathodal stimulation for the peaks ($P < 0.001$) and for the areas ($P < 0.01$ & $P < 0.001$ for 2 and 3 groups, respectively); and no significant effect after sham tsDCS. Similarly, the threshold crossings and knee points variables showed a significant increase (Figure 9, $P < 0.001$ & $P < 0.05$, respectively) after cathodal tsDCS and no significant effect after sham tsDCS.

As for the time domain approaches (Figure 10), the discharge rate showed a slight but non-significant increase for neither of the stimulation conditions. Likewise, the coefficient of variation of the FCC showed no significant change after cathodal/sham tsDCS. On the other hand, the coefficient of variation of the smoothed CST revealed a significant decrease after cathodal tsDCS and no significant effect after sham tsDCS. Similarly, the Z-scores of the correlation coefficients showed a significant decrease ($P < 0.05$ & $P < 0.001$ for 2 and 3 groups, respectively); and no significant effect after sham tsDCS.

IV. DISCUSSION

This study offers several approaches in time and frequency domain to analyze electrophysiological changes in MU activity due to cathodal tsDCS in incomplete SCI subjects. Moreover, an effective quality control algorithm is proposed for the automatic inspection of individual MU spike trains.

A significant decrease was found in the coherence between non-intersecting CSTs for all cases (peaks and areas with 2 and 3 groups of CSTs). These findings indicate a decrease in the common drive after cathodal stimulation was administered. Another evidence in support of this hypothesis was given by the fact that the number of MUs that contributes the

CSTs increased after cathodal tsDCS to reach a plateau in coherence (given by the knee point and threshold variables). In addition, the significant decrease of the cross-correlation peaks after cathodal tsDCS confirmed the findings in frequency domain.

Previous studies [34] indicated that the decorrelation between MU spike trains may be due to additional components of the synaptic input common to all MUs, but independent to the cortical drive. Namely, a secondary common input (e.g. enhanced sensory input) can decrease the strength of the common drive (reflected in the decrease of the coherence). Different experimental studies [35, 36] agree with this observation, suggesting an increase in the cross-correlation between spike trains during fatigue as a result of a decrease in afferent feedback. Concerning this study, the decrease in strength of the common drive after cathodal tsDCS is likely due to an increase of synaptic conductivity in afferent pathways as secondary common input.

Although no research had previously examined the effects of cathodal stimulation at the MU level, these findings are in line with similar studies in healthy subjects. Bocci et al. [16, 17] showed an increase in the MEP area and the motor unit recruitment after cathodal tsDCS, both indicating a facilitation of cortically elicited muscle actions. Similarly, facilitation after cathodal tsDCS has been reported by Ahmed and Wieraszko [18], who found an increase in the recruitment of larger MUs was found. Winkler et al. [19] suggested no significant influence on the excitability of the alpha-motor neuron after cathodal tsDCS, but an increase of the homosynaptic depression (possibly due to a hyperpolarization of Ia afferent membrane). Interestingly, a recent study [37] on SCI subjects suggested a laterality-dependent MEP response after

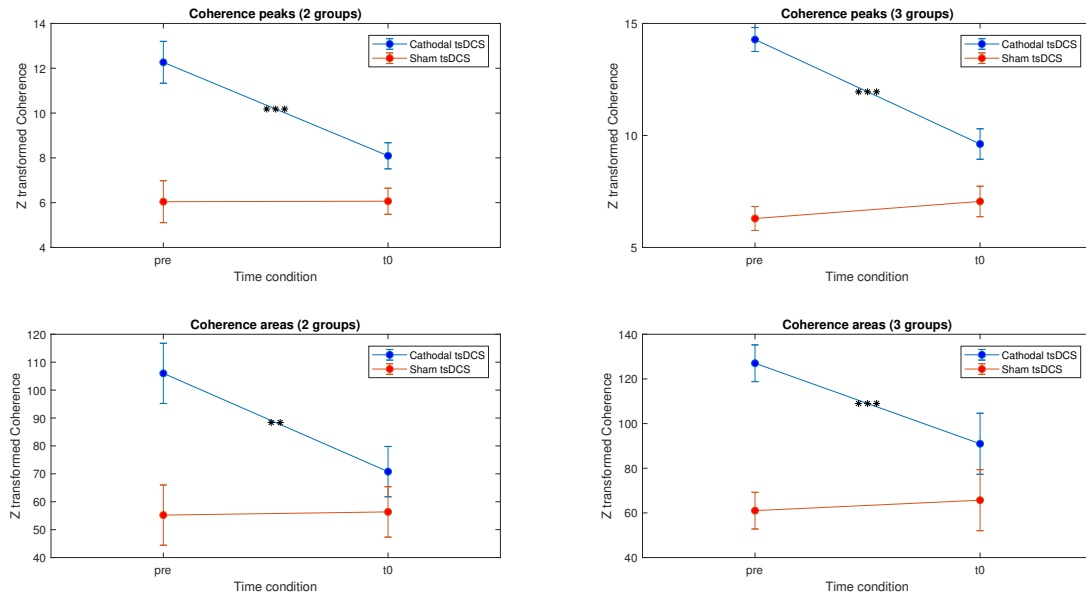


Fig. 8. The effects of cathodal (blue) and sham stimulation (red) on significant coherence peaks and area in the delta band (0-5 Hz). Error bars indicate the standard error of the mean. * $P < 0.05$, ** $P < 0.01$, and *** $P < 0.001$.

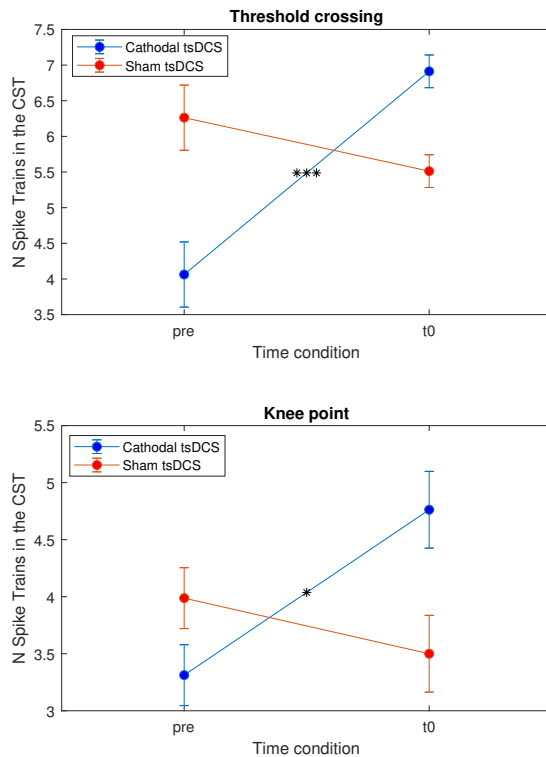


Fig. 9. Top figure: the effects of cathodal (blue) and sham stimulation (red) on the number of MUs required to reach a coherence peak of 0.9. Bottom figure: the effects of cathodal (blue) and sham stimulation (red) on the number of MUs of the knee point. The average of the coherence peaks was computed in the delta band (0-5 Hz). Error bars indicate the standard error of the mean. * $P < 0.05$, ** $P < 0.01$, and *** $P < 0.001$.

cathodal tsDCS. Particularly, the authors found an increase and a decrease in corticospinal excitability contralateral and ipsilateral to the reference electrode, respectively. However, this laterality response is not comparable to this study since no cortical stimulus was elicited.

Even though no significant effect was observed in the coefficient of variation of the FCC, the coefficient of variation of the smoothed CST showed a significant decrease after cathodal tsDCS. This discrepancy might be due to the fact that the FCC does not account for all the variation of the common drive. Although the FCC represents the greatest common variations of the instantaneous discharge rates of the motor neuron pool (FCC explained $46.6 \pm 10.7\%$ of the variability), relevant neural information could be comprised within the rest of the variation.

A decrease in the variability of the smoothed CST may indicate an improvement in force steadiness (decrease in the fluctuations of the common drive). However, the contradictory results of the FCC should not be totally disregarded considering chronic SCI. Due to the chronic phase of the injury in the subject, it is unlikely to observe substantial improvement in the steadiness of the common drive after a single session of stimulation. Moreover, multiple studies have not found a consensus on the relation between common drive and force fluctuations. Holtermann et al. [38] found the same trend (increase) in both, common input and force variability as the muscle fatigues but no association between them. In contrast, Contessa et al. [35] reported that the variability of the force was correlated to the common drive. However, they also found that the coefficient of variation of the firing rates was not related to the increase in variability of the force during fatigue. Therefore, a more conservative analysis

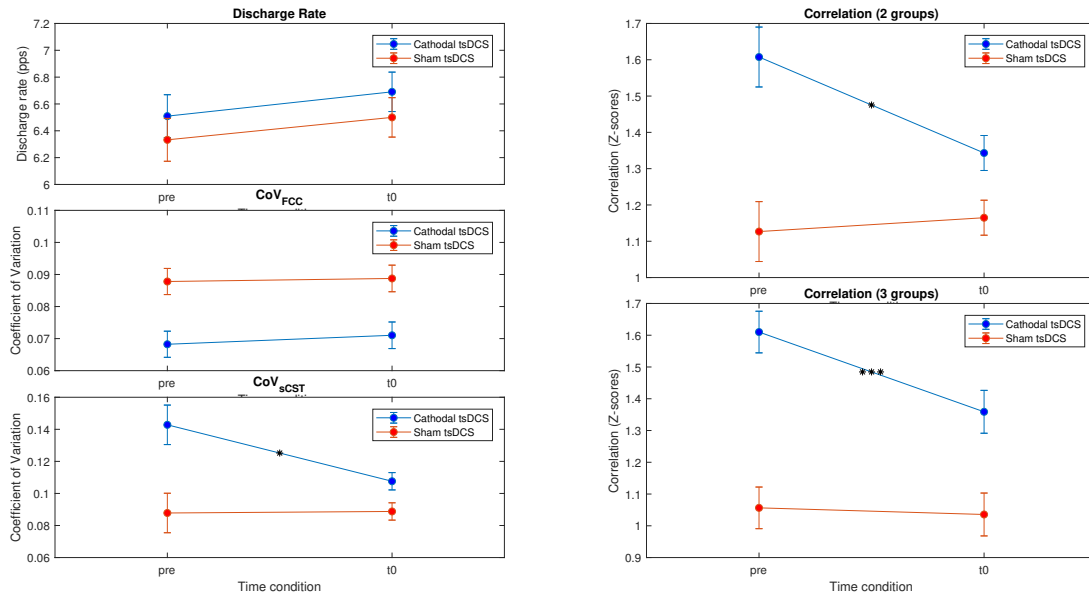


Fig. 10. The effects of cathodal (blue) and sham stimulation (red) on the average of the average discharge rate, coefficient of variation of the FCC and smoothed CST, and cross-correlation peaks. Error bars indicate the standard error of the mean. * $P < 0.05$, ** $P < 0.01$, and *** $P < 0.001$.

should be conducted taking into account force measurements and a MU-tracking methodology as proposed by Martinez-Valdes et al. [28].

The most substantial methodological issue of this study is the lack of statistical power due to the sample size. As only one subject was analyzed, a two-way repeated measures ANOVA test was disregarded. With 8 repetitions, most of the variables only had 7 degrees of freedom (df), and the variables split into three groups had 23 df. For this reason, a rate of consistency was included in Table III (Appendix C) to stress that not only the means were significantly different, but also the trends were consistent across all or almost all repetitions (7/8 & $> 21/24$).

As mentioned before, another issue is the lack of a MU-tracking methodology as proposed by Martinez-Valdes et al. [28]. Having a decomposition of the same MUs across experimental trials may be helpful to find significant differences in the discharge rates after cathodal stimulation as well as to confirm a decrease in variability with the FCC. Additionally, it may improve the methodology in frequency domain. This applies especially to the second approach, in which the significant increase in MUs reaching a plateau in coherence after cathodal tsDCS may be biased by the difference between the amount of MUs identified in each time condition. As it is uncertain whether the same MUs are being compared, this limitation may also account for the differences of the mean values before stimulation between the cathodal and sham experiments (Figure 8, 9, and 7).

Moreover, identifying the same MUs across trials may be useful to build predictive models with ISIs and PCA transformations of spike trains as inputs. Research in neural information processing has revealed accurate classification

of neural activity states (e.g. REM states), neuron cell types (e.g. inhibitory and excitatory) [39], and spoken words (e.g. "zero", "one", "two") [40]. These methodologies can be replicated in the field of neuromodulation to optimize stimulation parameters at a later stage.

Further improvement in this methodology includes a detailed validation of the decomposition as proposed by Negro et al. [30]. In particular, identifying individual mismatched spikes would avoid the need of eliminating some entire MU spike trains in the quality control. As a result, less neural information would be compromised. However, this would make the experimental set-up more complicated as it requires not only surface EMG but also intramuscular EMG recordings.

With respect to the experimental set-up, targeting more accurately specific spinal cord segments can increase the effects of cathodal tsDCS. As shown in Figure 13 (Appendix A), administering cathodal tsDCS in between the 11th and 12th thoracic vertebrae ($\sim L3-L5$ of spinal cord segments) can barely stimulate the motor neuron pools of the soleus muscle ($\sim L5-S2$) and the stimulation may not reach the medialis gastrocnemius. This explains why no consistent visual behaviour was found in the gastrocnemius during earlier stages of the project. Whereas this configuration may have a major impact on the vastus lateralis, tibialis anterior and hamstrings muscles, placing the electrode one vertebra lower ($\sim L5-S3$ of the spinal cord segments) would influence more the soleus and gastrocnemius. Furthermore, the protocol could be expanded to include healthy subjects and anodal tsDCS, which has been proven to have significant effects on different mechanisms of the spinal cord [16, 17].

TABLE II

NORMALITY AND STUDENT'S PAIRED T-TESTS FOR EACH VARIABLE.
 VARIABLES WITH SIGNIFICANT EFFECTS ARE HIGHLIGHTED WITH A
 LIGHT GRAY BACKGROUND: *P < 0.05, **P < 0.01, AND ***P < 0.001.

Dependent variable	Type of tsDCS	Time	Shapiro Wilk			Paired t-test		
			W	df	p-value	t	df	p-value
Coherence Peaks (2 groups)	Cathodal	pre t0	0.96 0.97	8 8	0.758 0.925	6.15	7	0.000***
	Sham	pre t0	0.95 0.92	8 8	0.705 0.458	-0.03	7	0.980
Coherence Peaks (3 groups)	Cathodal	pre t0	0.98 0.98	24 24	0.853 0.865	7.89	23	0.000***
	Sham	pre t0	0.96 0.95	24 24	0.474 0.264	-0.44	23	0.664
Coherence Areas (2 groups)	Cathodal	pre t0	0.95 0.92	8 8	0.664 0.224	4.79	7	0.002**
	Sham	pre t0	0.85 0.91	8 8	0.103 0.325	-0.09	7	0.927
Coherence Areas (3 groups)	Cathodal	pre t0	0.98 0.92	24 24	0.815 0.062	5.10	23	0.000***
	Sham	pre t0	0.97 0.93	24 24	0.678 0.104	-0.99	23	0.332
Threshold	Cathodal	pre t0	0.98 0.98	8 8	0.964 0.979	-7.04	7	0.000***
	Sham	pre t0	0.84 0.96	8 8	0.080 0.774	1.38	7	0.209
Knee point	Cathodal	pre t0	0.89 0.96	8 8	0.251 0.851	-2.85	7	0.025*
	Sham	pre t0	0.97 0.80	8 8	0.912 0.030*	1.00	-	-
Knee point (logarithm)	Cathodal	pre t0	0.94 0.94	8 8	0.584 0.654	-2.86	7	0.024*
	Sham	pre t0	0.93 0.84	8 8	0.520 0.082	0.73	7	0.490
Average discharge rate	Cathodal	pre t0	0.94 0.87	8 8	0.620 0.155	-1.24	7	0.254
	Sham	pre t0	0.89 0.94	8 8	0.245 0.563	-1.45	7	0.189
CoV FCC	Cathodal	pre t0	0.94 0.96	8 8	0.606 0.826	-0.50	7	0.634
	Sham	pre t0	0.97 0.98	8 8	0.884 0.955	-0.11	7	0.915
CoV smoothed CST	Cathodal	pre t0	0.93 0.90	8 8	0.531 0.292	3.20	7	0.015*
	Sham	pre t0	0.97 0.98	8 8	0.884 0.955	-0.11	7	0.915
Correlation smoothed CST (2 groups)	Cathodal	pre t0	0.98 0.90	8 8	0.974 0.259	2.53	7	0.039*
	Sham	pre t0	0.90 0.89	8 8	0.298 0.252	-0.42	7	0.686
Correlation smoothed CST (3 groups)	Cathodal	pre t0	0.98 0.95	24 24	0.886 0.206	4.35	23	0.000***
	Sham	pre t0	0.96 0.93	24 24	0.4 0.075	-0.92	23	0.367

Considering the lack of participants in the protocol, no definite conclusion can be ascertained. Nonetheless, this study suggests that the common drive decreases immediately after cathodal tsDCS which is reflected in the decrease in coherence within the delta band, the decorrelation between smoothed CSTs, and the increase of the amount of MUs required to reach a plateau in coherence. This implies an enhanced sensory feedback as secondary common input. After further validation of these findings on more SCI patients and healthy subjects, these features could be used as biomarkers in a follow-up study to optimize stimulation parameters and to design a closed-loop modulation strategy for the corticospinal excitability.

ACKNOWLEDGMENT

I would like to express my deepest gratitude to Dr. Massimo Sartori and Dr. Utku Yavuz for their insightful guidance and encouragement throughout my master's thesis. I would also like to thank Dr. Jan Buitenweg for his additional support and valuable advice.

APPENDIX A: BACKGROUND

Anatomy of the Spinal Cord

The spinal cord is a bundle of nerve tissue that extends caudally from the brainstem to the 2nd lumbar vertebra [41]. It is protected by the vertebral column and three surrounding layers of tissue, and constitutes together with the brain the central nervous system (CNS). The spinal cord tissue comprises gray and white matter. The gray matter, consisting mainly of neuronal body cells (soma), is located in the center; the white matter surrounds the gray matter and contains mainly myelinated axons and glial cells. The spinal cord is divided into 31 segments: 8 cervical (C1-C8), 12 thoracic (T1-T12), 5 lumbar (L1-L5), 5 sacral (S1-S5), and 1 coccygeal. Figure 11 depicts the relation of the spinal cord segments to vertebrae. From each segment, two bilateral spinal nerves emerge by ventral and dorsal roots. The former are composed of motor fibers and the latter of sensory fibers (Figure 12).

The major functions of the spinal cord are to carry out motor and somatosensory information between the brain and the peripheral nervous system (PNS) as well as to coordinate some simple reflexes (involuntary responses to outside stimuli). For locomotion, motor commands are sent from the cerebral cortex (primary motor cortex) by upper motor neurons. The axon of the upper motor neuron descends through the spinal cord and synapses with an interneuron or directly with an alpha-motor neuron. The axon of the alpha-motor neuron arises from the spinal cord in a nerve and innervates several muscle fibers. An alpha-motor neuron and the fibers it innervates constitute a motor unit. A motor neuron pool is composed of all motor units that innervate a single muscle. The neural circuits related to the lower extremities function arise from the lumbosacral segments. Figure 13 shows the approximate location of the motor neuron pools responsible for the innervation of the medial gastrocnemius (MG), soleus (SOL), tibialis anterior (TA), medial hamstrings (MH) and vasti lateralis (VL) according to Kendall et al. [41]. Thus, the lumbosacral spinal cord, located approximately between the T10 and L2 vertebrae, is the main target of tsDCS to modulate abnormal behavior of neural activity due to motor dysfunction on the lower limbs.

Common synaptic input and motor function

The simplified model for the generation of the effective neural drive to the muscle comprises independent inputs (independent noise) and common inputs (inputs that are the same for the entire motor pool) [10, 11, 14, 30] (Figure 14). The independent input approximates the behavior of individual membrane fluctuations (e.g. ion channel noise) [10]. On the other hand, the common input consists of a control input,

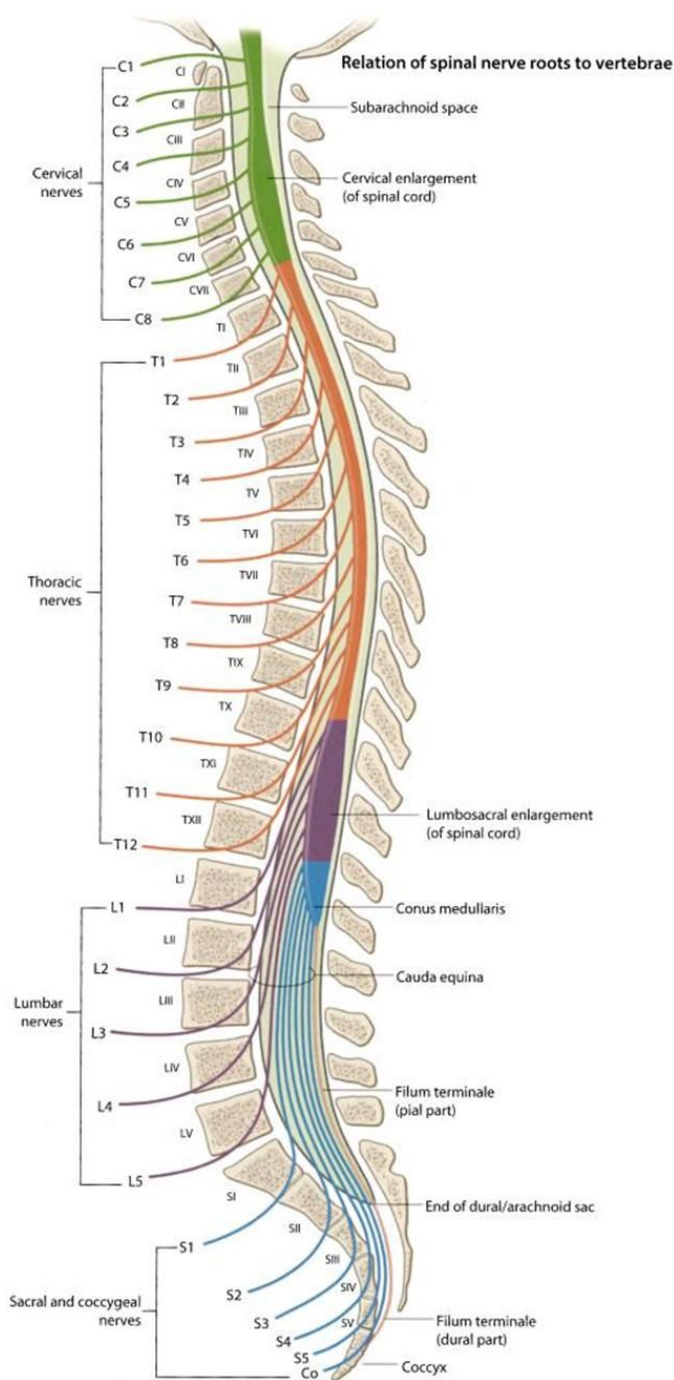


Fig. 11. Relation of spinal nerve roots to vertebrae. The vertebrae are numbered with roman numerals and the spinal cord nerves (segments) with Arabic numerals. Adapted from Drake et al. [42].

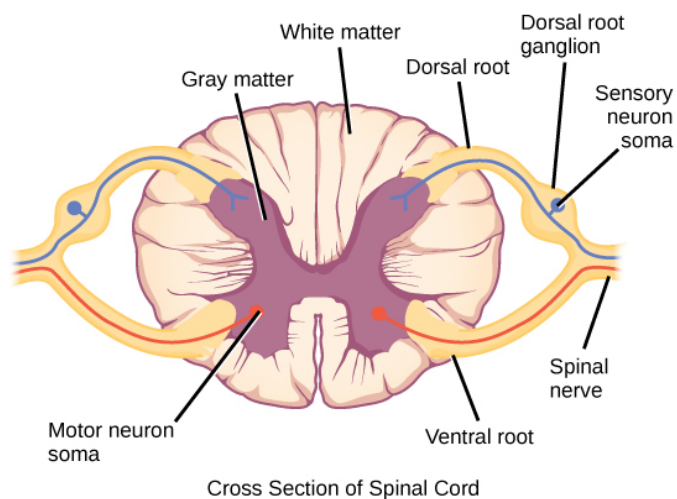


Fig. 12. Spinal cord cross-section. Spinal cord tissue is mainly composed of gray matter (body cells, in the center) and white matter (axons, surrounding the gray matter). Dorsal roots consist of afferent neurons (sensory neuron in blue) and ventral roots consist of efferent neurons (motor neurons in red). Both unite to form the spinal nerve and exchange information with the periphery. Adapted from <https://www.newhealthadvisor.com>

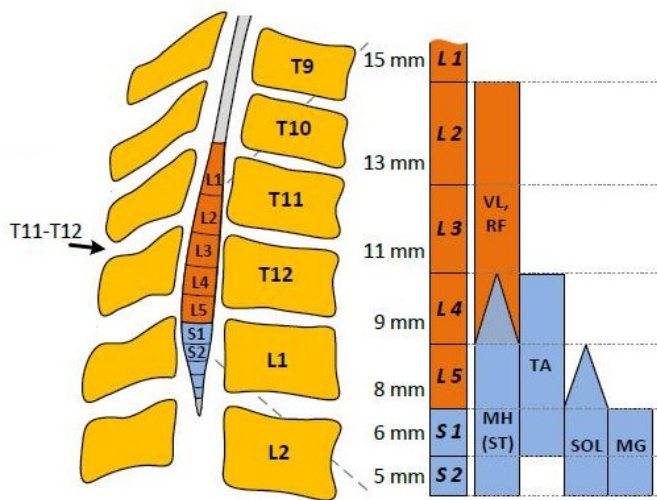


Fig. 13. Enlargement of the lumbosacral spinal cord. The tsDCS is administered approximately between the 11th and 12th vertebrae (~L3-L5 spinal segments). On the right, a scheme is displayed with the approximate location of the motor neuron pools based on the segmental charts provided by Kendall et al. [41]. These charts are a compilation of six clinical well-known sources. The triangle endings denote agreement of three or four sources; the square endings denote a strong agreement (five or all sources). The measures depicted to the left of each segment are the average length in millimeters of the segment [43]. Adapted from Sayenko et al. [44].

also known as common drive, and common noise. The former regulates the force and the latter determines the oscillations of the neural drive to the muscle around the target force [14]. The common input is approximately given by the low frequency components (<10 Hz) of the CST (sum of MU spike trains), from which the common drive approximates to the very low frequency bandwidth (delta band, <5 Hz) [10].

For this reason, the common input is of key importance for studying motor function. In particular, the strength of the common drive can be obtained by measuring the correlation between two CSTs that comprise several MUs. The magnitude-squared coherence, or simply coherence, is an analogue measure of the cross-correlation in frequency domain. It allows to distinguish the strength of linear relationship between two signals within different bandwidths. As the delta bandwidth is of particular interest for understanding voluntary movement, coherence analysis is useful to (roughly) measure the strength of the common drive.

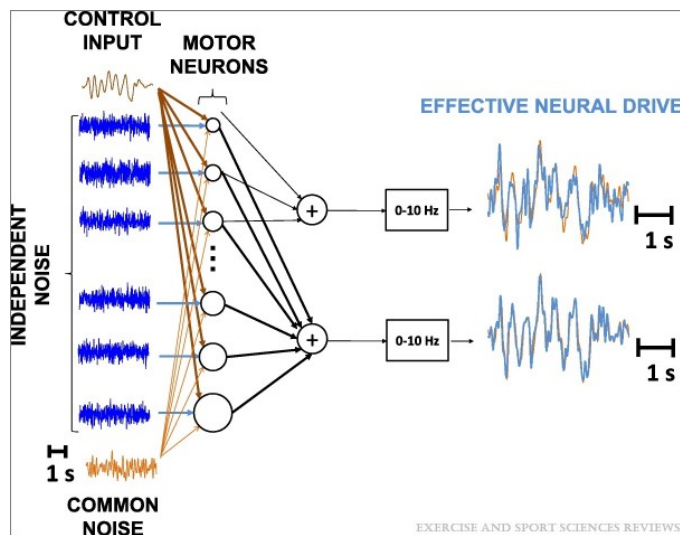


Fig. 14. Simplified model for the generation of the effective neural drive to the muscle. The common drive (for force control) and common noise (related to oscillations of the neural drive to the muscle) are distributed to all motor neurons. Additionally, each motor neuron receives an independent input (independent noise). On the right, a comparison between the effective neural drive (in blue) and the low frequency component of the CST (<10 Hz, in red) is shown. The upper CST includes three motor neurons, whereas the lower CST includes all the motor neurons in the pool. Adapted from Farina and Negro [14].

Trans-spinal direct current stimulation

Trans-spinal direct current stimulation (tsDCS) is a non-invasive technique for the modulation of the spinal cord function. It is administered by an electrical stimulator with two superficial electrodes on the skin (at the target spinal segment). Low direct current (<2.5 mA) is delivered to the target spinal segment, generating an electric field (from anode to cathode). The electric field induces a de- or hyperpolarization to the neural circuitry (including motor neurons, sensory axons and corticospinal axons [Figure 15]) depending on the polarity of the electrode configuration (cathodal or anodal). Among other stimulation parameters that have

a major influence on corticospinal excitability are the electrode position, current intensity and stimulus waveform [45]. Conventionally, the reference electrode is placed on one of the deltoids (muscle responsible for the range of motion of the shoulder) and the active electrode centered between the vertebrae related to target spinal segments of interest. For instance, targeting the lumbrosacral segments of the spinal cord (Figure 13) stimulates mostly the lower extremities muscles. Moreover, altering the intensity also changes the effect of the modulation. Whereas higher stimulation intensity can directly evoke action potentials, lower stimulation intensity influences neural activation without directly evoking any action potential [45].

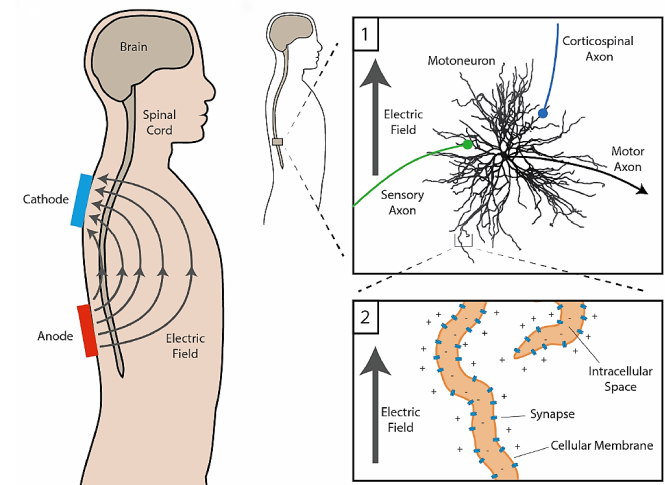


Fig. 15. Overview of tsDCS. On the left: The stimulation induces an electric field from anode to cathode. On the right: (1) The electric field interacts with complex neural circuits including motoneurons, sensory axons and corticospinal axons. (2) A microscopic view of the complex structures shows a cable-like geometry. Adapted from Kuck [45]

In order to assess electrophysiological changes generated by tsDCS, classic techniques to test (indirectly) the excitability of motor neuron pools and corticospinal excitability can be performed. These techniques measure evoked compound muscle action potentials elicited from external stimuli. The H-reflex (Hoffman-reflex) is a reflex response evoked by electrical stimulation of a peripheral nerve [22]. It is the electrical analogue to the stretch reflex. The electrical stimulus is administered on sensory fibers which generates an action potential in sensory and motor axons. An M-wave (early, low-amplitude response) is generated directly from the activation of alpha-motor neurons by the electrical stimulus, while the action potential travels from the sensory fibers to the spinal cord and activates alpha motor neurons. Subsequently, the signal travels back to the muscle along the axon of the alpha motor neuron, evoking an H-wave. Whereas this method can be relatively simple and painless, it is also affected by post-activation depression and changes in axonal excitability [22,23]. On the other hand, the F-wave is generated by provoking an antidromic (travelling in the opposite direction of the fiber) activation of the motor neu-

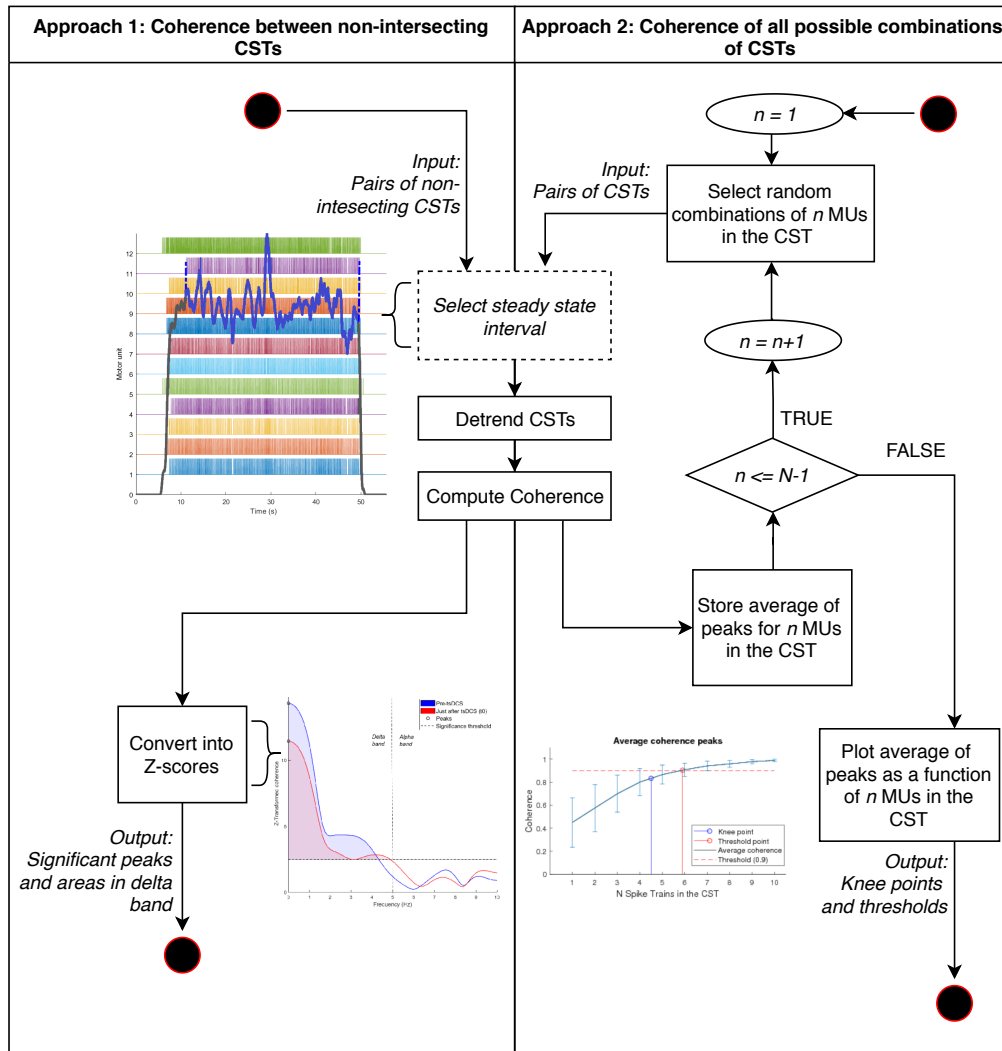


Fig. 16. Flow diagram of the approaches in frequency domain. The black circles with red contour represent the start and the end of each approach. The square with dashed lines denotes a sub-algorithm for selecting the steady state interval (Figure 18).

rons with a strong electrical stimulus. The main advantage of this method is that it does not involve afferent feedback, however, it can be painful and relatively insensitive to motor neuron excitability [22]. MEPs are elicited in peripheral muscles by transcranial magnetic stimulation (TMS) over human motor cortex (multiple impulses descending in the corticospinal tract). This method offers a reliable measure of corticospinal excitability, nevertheless, their interpretation is limited as cortical and spinal excitability cannot be analyzed in isolation [22].

APPENDIX B: DIAGRAMS OF APPROACHES

Figure 16 shows a flowchart for the approaches in frequency domain: coherence between non-intersecting CSTs (subsection II-D) and average of coherence peaks of all possible combinations (subsection II-E). Figure 18 illustrates a flowchart for the approaches in time domain (subsection II-F). Figure 17 depicts a flowchart for the algorithm to obtain the steady state interval, in which all motor units are concurrently active.

APPENDIX C: SUMMARY OF RESULTS

Table III summarizes the results for each variable. It includes the means, standard deviations, standard error means and rates of consistency (number of repetitions following the same trend divided by the total sample size).

The files of this thesis are divided into two folders: *Results* and *Scripts and data*. The folder *Results* contains an Excel workbook with two main worksheets: Final STATS and Final results. Additionally, this folder contains a file with the datasets in SPSS and the syntax for the statistical tests.

The folder *Scripts and data* contains the Matlab scripts for each approach, a read.tex file with additional instructions, and the folders with the data of each SCI subject. The folders of the SCI subjects are organized as follows:

- *Injured*. Subject 1, raw and decomposed files: experiment 1 = sham & experiment 2 = cathodal.
- *Injured2*. Subject 2, raw and decomposed files: experiment 1 = cathodal (poor data quality) & experiment 2 = sham

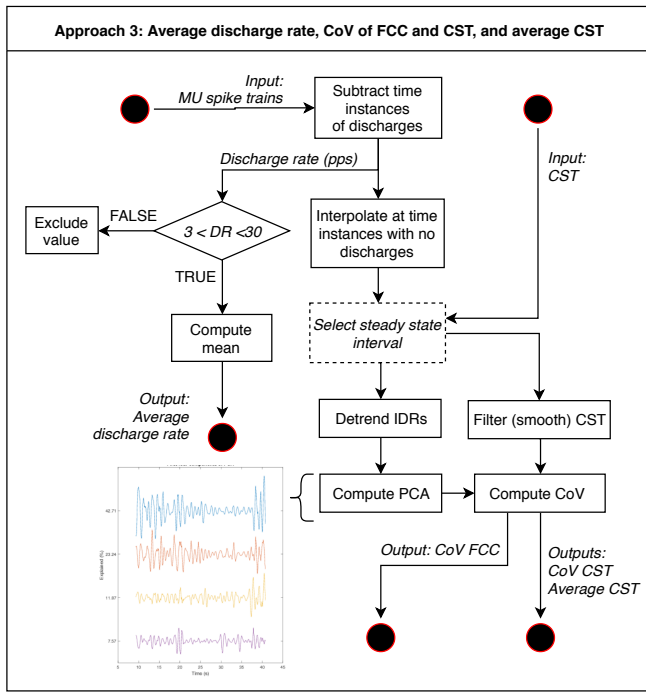


Fig. 17. Flow diagram of the approaches in time domain. The black circles with red contour represent the start and the end of each approach. The square with dashed lines denotes a sub-algorithm for selecting the steady state interval (Figure 18).

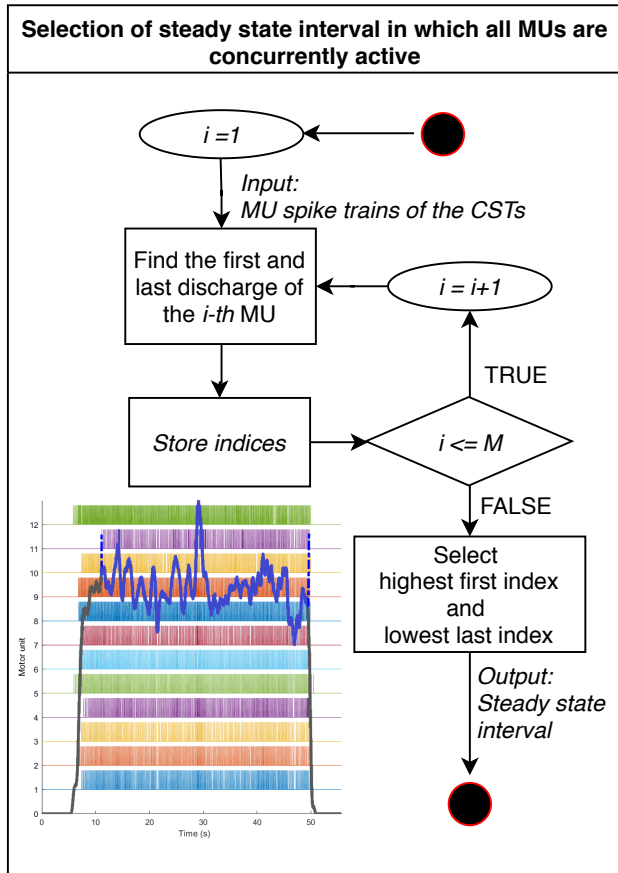


Fig. 18. Flow diagram of the sub-algorithm for selecting the steady state interval. The black circles with red contour represent the start and the end of the algorithm.

- *Injured3*. Subject 3, raw and decomposed files: experiment 1 = cathodal & experiment 2 = sham (poor data quality in both).
- *Injured4*. Subject 4, only raw files: experiment 1 = sham & experiment 2 = cathodal. It is not decomposed because there was a change in the protocol with this subject (half of the intensity of the stimulation).

TABLE III

SUMMARY OF RESULTS. VARIABLES WITH SIGNIFICANT EFFECTS ARE HIGHLIGHTED WITH LIGHT GRAY BACKGROUND. SD STANDS FOR STANDARD DEVIATION, SEM FOR STANDARD ERROR MEAN. THE RATE OF CONSISTENCY IS ONLY GIVEN FOR VARIABLES WITH SIGNIFICANT EFFECTS. PLUS (+) AND MINUS SIGNS (-) IN PARENTHESIS REPRESENT INCREASING AND DECREASING TRENDS, RESPECTIVELY.

Dependent variable	Type of tDCS	Time	Mean	N	SD	SEM	Consistency Rate	Trend
<i>Coherence Peaks</i> (2 groups)	Cathodal	pre	12.27	8	2.65	0.94	8/8	(-)
	t0	8.09	8	1.65	0.58			
<i>Coherence Peaks</i> (3 groups)	Sham	pre	6.04	8	1.86	0.66	-	-
	t0	6.06	8	1.05	0.37			
<i>Coherence Areas</i> (2 groups)	Cathodal	pre	13.34	24	2.49	0.51	23/24	(-)
	t0	8.77	24	1.78	0.36			
<i>Coherence Areas</i> (3 groups)	Sham	pre	5.61	24	2.10	0.43	-	-
	t0	5.88	24	2.03	0.41			
<i>Coherence Areas</i> (2 groups)	Cathodal	pre	55.22	8	21.78	7.70	8/8	(-)
	t0	56.36	8	21.10	7.46			
<i>Coherence Areas</i> (3 groups)	Sham	pre	105.99	8	30.50	10.78	-	-
	t0	70.78	8	25.52	9.02			
<i>Coherence Areas</i> (3 groups)	Cathodal	pre	114.37	24	34.46	7.03	23/24	(-)
	t0	71.69	24	30.79	6.28			
<i>Threshold</i>	Sham	pre	44.37	24	23.83	4.87	-	-
	t0	51.75	24	26.93	5.50			
<i>Threshold</i>	Cathodal	pre	4.06	8	1.29	0.46	8/8	(+)
	t0	6.91	8	0.65	0.23			
<i>Knee point</i>	Sham	pre	6.26	8	1.10	0.39	-	-
	t0	5.51	8	0.79	0.28			
<i>Knee point</i>	Cathodal	pre	3.31	8	0.75	0.27	5/8	(+)
	t0	4.76	8	0.95	0.34			
<i>Knee point (logarithm)</i>	Sham	pre	3.99	8	1.18	0.42	-	-
	t0	3.50	8	0.50	0.18			
<i>Average discharge rate</i>	Cathodal	pre	0.511	8	0.092	0.033	5/8	(+)
	t0	0.670	8	0.092	0.032			
<i>Average discharge rate</i>	Sham	pre	0.582	8	0.142	0.050	-	-
	t0	0.541	8	0.057	0.020			
<i>CoV FCC</i>	Cathodal	pre	6.51	8	0.45	0.16	-	-
	t0	6.69	8	0.42	0.15			
<i>CoV FCC</i>	Sham	pre	6.33	8	0.66	0.24	-	-
	t0	6.50	8	0.63	0.22			
<i>CoV smoothed CST</i>	Cathodal	pre	0.068	8	0.012	0.004	-	-
	t0	0.071	8	0.012	0.004			
<i>CoV smoothed CST</i>	Sham	pre	0.088	8	0.020	0.007	-	-
	t0	0.089	8	0.025	0.009			
<i>Correlation smoothed CST</i> (2 groups)	Cathodal	pre	0.143	8	0.035	0.012	8/8	(-)
	t0	0.108	8	0.015	0.005			
<i>Correlation smoothed CST</i> (2 groups)	Sham	pre	0.088	8	0.020	0.007	-	-
	t0	0.089	8	0.025	0.009			
<i>Correlation smoothed CST</i> (3 groups)	Cathodal	pre	1.61	8	0.23	0.08	7/8	(-)
	t0	1.34	8	0.14	0.05			
<i>Correlation smoothed CST</i> (3 groups)	Sham	pre	1.13	8	0.15	0.05	-	-
	t0	1.16	8	0.19	0.07			
<i>Correlation smoothed CST</i> (3 groups)	Cathodal	pre	1.52	24	0.24	0.05	21/24	(-)
	t0	1.25	24	0.19	0.04			
<i>Correlation smoothed CST</i> (3 groups)	Sham	pre	0.97	24	0.18	0.04	-	-
	t0	1.02	24	0.19	0.04			

REFERENCES

- [1] A. Kuck, H. van der Kooij, D. Stegeman, and E. F. van Asseldonk, "Effect of trans-spinal-direct current stimulation on force and emg output during isometric contractions," To appear, unpublished protocol.
- [2] V. Dietz and A. Curt, "Neurological aspects of spinal-cord repair: promises and challenges," *Lancet neurology*, vol. 5, pp. 688–94, 09 2006.
- [3] M. P. Jensen, C. M. Kuehn, D. Amtmann, and D. Cardenas, "Symptom burden in persons with spinal cord injury," *Archives of physical medicine and rehabilitation*, vol. 88, pp. 638–45, 06 2007.
- [4] A. Singh, L. Tetreault, S. Kalsi-Ryan, A. Nouri, and M. Fehlings, "Global prevalence and incidence of traumatic spinal cord injury: clinical epidemiology," *Clinical epidemiology*, vol. 6, pp. 309–31, 2014.
- [5] J. H. Nijendijk, M. W. Post, and F. W. van Asbeck, "Epidemiology of traumatic spinal cord injuries in the netherlands in 2010," *Spinal Cord*, vol. 52, p. 258, 2014.
- [6] R. Nardone, Y. Hiller, F. Brigo, M. Seidl, M. Christova, J. Bergmann, S. Golaszewski, and E. Trinka, "Functional brain reorganization after spinal cord injury: Systematic review of animal and human studies," *Brain Research*, vol. 1504, pp. 58 – 73, 2013. [Online]. Available: <http://www.sciencedirect.com/science/article/pii/S0006899312019695>
- [7] R. Nardone, Y. Hiller, A. Thomschewski, A. Bathke, A. R. Ellis, S. Golaszewski, F. Brigo, and E. Trinka, "Assessment of corticospinal excitability after traumatic spinal cord injury using mep recruitment curves: a preliminary tms study," *Spinal Cord*, vol. 53, p. 534, 2015.
- [8] C. K. Thomas, R. Bakels, C. S. Klein, and I. Zijdwind, "Human spinal cord injury: motor unit properties and behaviour," *Acta Physiologica*, vol. 210, no. 1, pp. 5–19, 2014. [Online]. Available: <https://onlinelibrary.wiley.com/doi/abs/10.1111/apha.12153>
- [9] F. Negro and D. Farina, "Factors influencing the estimates of correlation between motor unit activities in humans," *PLOS ONE*, vol. 7, no. 9, pp. 1–14, 09 2012. [Online]. Available: <https://doi.org/10.1371/journal.pone.0044894>
- [10] F. Negro, U. Yavuz, and D. Farina, "The human motor neuron pools receive a dominant slow-varying common synaptic input," *The Journal of Physiology*, vol. 594, no. 19, pp. 5491–5505, 2016. [Online]. Available: <https://physoc.onlinelibrary.wiley.com/doi/abs/10.1113/JP271748>
- [11] D. G. Lawrence, R. Porter, and S. J. Redman, "Corticospinal synapses in the monkey: Light microscopic localization upon motoneurons of intrinsic muscles of the hand," *Journal of Comparative Neurology*, vol. 232, no. 4, pp. 499–510, 1985. [Online]. Available: <https://onlinelibrary.wiley.com/doi/abs/10.1002/cne.902320407>
- [12] C. J. D. Luca and W. J. Forrest, "An electrode for recording single motor unit activity during strong muscle contractions," *IEEE Transactions on Biomedical Engineering*, vol. BME-19, no. 5, pp. 367–372, Sep. 1972.
- [13] H. P. Clamann, "Activity of single motor units during isometric tension," *Neurology*, vol. 20, no. 3, pp. 254–254, 1970. [Online]. Available: <http://n.neurology.org/content/20/3/254>
- [14] D. Farina and F. Negro, "Common synaptic input to motor neurons, motor unit synchronization, and force control." *Exercise and sport sciences reviews*, vol. 43, 11 2014.
- [15] C. De Luca and Z. Erim, "Common drive of motor units in regulation of muscle force," *Trends in neurosciences*, vol. 17, pp. 299–305, 08 1994.
- [16] T. Bocci, S. Marceglia, M. Vergari, V. Cognetto, F. Cogliamian, F. Sartucci, and A. Priori, "Transcutaneous spinal direct current stimulation modulates human corticospinal system excitability," *Journal of Neurophysiology*, vol. 114, no. 1, pp. 440–446, 2015, pMID: 25925328. [Online]. Available: <https://doi.org/10.1152/jn.00490.2014>
- [17] T. Bocci, B. Vannini, A. Torzini, A. Mazzatenta, M. Vergari, F. Cogliamian, A. Priori, and F. Sartucci, "Cathodal transcutaneous spinal direct current stimulation (tsdcs) improves motor unit recruitment in healthy subjects," *Neuroscience Letters*, vol. 578, pp. 75 – 79, 2014. [Online]. Available: <http://www.sciencedirect.com/science/article/pii/S0304394014005187>
- [18] Z. Ahmed and A. Wieraszko, "Trans-spinal direct current enhances corticospinal output and stimulation-evoked release of glutamate analog, d-2,3-h-3-aspartic acid," *Journal of applied physiology (Bethesda, Md. : 1985)*, vol. 112, pp. 1576–92, 02 2012.
- [19] T. Winkler, P. Hering, and A. Straube, "Spinal dc stimulation in humans modulates post-activation depression of the h-reflex depending on current polarity," *Clinical Neurophysiology*, vol. 121, no. 6, pp. 957 – 961, 2010. [Online]. Available: <http://www.sciencedirect.com/science/article/pii/S1388245710000544>
- [20] F. Cogliamian, M. Vergari, F. Pulecchi, S. Marceglia, and A. Priori, "Effect of spinal transcutaneous direct current stimulation on somatosensory evoked potentials in humans," *Clinical neurophysiology : official journal of the International Federation of Clinical Neurophysiology*, vol. 119, pp. 2636–40, 10 2008.
- [21] F. Cogliamian, M. Vergari, E. Schiaffini, S. Marceglia, G. Ardolino, S. Barbieri, and A. Priori, "Transcutaneous spinal cord direct current stimulation inhibits the lower limb nociceptive flexion reflex in human beings," *PAIN*, vol. 152, no. 2, pp. 370 – 375, 2011. [Online]. Available: <http://www.sciencedirect.com/science/article/pii/S0304395910006755>
- [22] C. J. McNeil, J. Butler, J. Taylor, and S. Gandevia, "Testing the excitability of human motoneurons," *Frontiers in human neuroscience*, vol. 7, p. 152, 04 2013.
- [23] H. Hultborn and J. B. Nielsen, "H-reflexes and f-responses are not equally sensitive to changes in motoneuronal excitability," *Muscle & Nerve*, vol. 18, no. 12, pp. 1471–1474, 1995. [Online]. Available: <https://onlinelibrary.wiley.com/doi/abs/10.1002/mus.880181219>
- [24] J. L. Dideriksen, F. Negro, D. Falla, S. R. Kristensen, N. Mrachacz-Kersting, and D. Farina, "Coherence of the surface emg and common synaptic input to motor neurons," *Frontiers in Human Neuroscience*, vol. 12, p. 207, 2018. [Online]. Available: <https://www.frontiersin.org/article/10.3389/fnhum.2018.00207>
- [25] C. M. Laine, E. Martinez-Valdes, D. Falla, F. Mayer, and D. Farina, "Motor neuron pools of synergistic thigh muscles share most of their synaptic input," *Journal of Neuroscience*, vol. 35, no. 35, pp. 12207–12216, 2015. [Online]. Available: <http://www.jneurosci.org/content/35/35/12207>
- [26] F. Negro, A. Holobar, and D. Farina, "Fluctuations in isometric muscle force can be described by one linear projection of low-frequency components of motor unit discharge rates," *The Journal of Physiology*, vol. 587, no. 24, pp. 5925–5938, 2009. [Online]. Available: <https://physoc.onlinelibrary.wiley.com/doi/abs/10.1113/jphysiol.2009.178509>
- [27] A. Holobar, M. A. Minetto, and D. Farina, "Accurate identification of motor unit discharge patterns from high-density surface emg and validation with a novel signal-based performance metric," *Journal of Neural Engineering*, vol. 11, no. 1, p. 016008, 2014. [Online]. Available: <http://stacks.iop.org/1741-2552/11/i=1/a=016008>
- [28] E. Martinez-Valdes, F. Negro, C. M. Laine, D. Falla, F. Mayer, and D. Farina, "Tracking motor units longitudinally across experimental sessions with high-density surface electromyography," *The Journal of Physiology*, vol. 595, no. 5, pp. 1479–1496, 2017. [Online]. Available: <https://physoc.onlinelibrary.wiley.com/doi/abs/10.1113/JP273662>
- [29] C. Pollock, T. Ivanova, M. Hunt, and S. Garland, "Behavior of medial gastrocnemius motor units during postural reactions to external perturbations after stroke," *Clinical Neurophysiology*, vol. 126, no. 10, pp. 1951 – 1958, 2015. [Online]. Available: <http://www.sciencedirect.com/science/article/pii/S1388245714008591>
- [30] F. Negro, S. Muceli, A. M. Castronovo, A. Holobar, and D. Farina, "Multi-channel intramuscular and surface emg decomposition by convolutive blind source separation," *Journal of Neural Engineering*, vol. 13, no. 2, p. 026027, 2016. [Online]. Available: <http://stacks.iop.org/1741-2552/13/i=2/a=026027>
- [31] A. Holobar, D. Farina, M. Gazzoni, R. Merletti, and D. Zazula, "Estimating motor unit discharge patterns from high-density surface electromyogram," *Clinical Neurophysiology*, vol. 120, no. 3, pp. 551 – 562, 2009. [Online]. Available: <http://www.sciencedirect.com/science/article/pii/S1388245709000030>
- [32] J. Rosenberg, A. Amjad, P. Breeze, D. Brillinger, and D. Halliday, "The fourier approach to the identification of functional coupling between neuronal spike trains," *Progress in Biophysics and Molecular Biology*, vol. 53, no. 1, pp. 1 – 31, 1989. [Online]. Available: <http://www.sciencedirect.com/science/article/pii/0079610789900047>
- [33] C. J. de Luca, R. S. LeFever, M. P. McCue, and A. P. Xenakis, "Control scheme governing concurrently active human motor units during voluntary contractions," *The Journal of Physiology*, vol. 329, no. 1, pp. 129–142, 1982. [Online]. Available: <https://physoc.onlinelibrary.wiley.com/doi/abs/10.1113/jphysiol.1982.sp014294>
- [34] F. Negro and D. Farina, "Decorrelation of cortical inputs and motoneuron output," *Journal of neurophysiology*, vol. 106, pp. 2688–97, 07 2011.
- [35] P. Contessa, A. Adam, and C. J. De Luca, "Motor unit control and force fluctuation during fatigue," *Journal of Applied Physiology*, vol.

- 107, no. 1, pp. 235–243, 2009, PMID: 19390005. [Online]. Available: <https://doi.org/10.1152/jappphysiol.00035.2009>
- [36] C. De Luca, “Myoelectrical manifestations of localized muscular fatigue in humans,” *Critical reviews in biomedical engineering*, vol. 11, pp. 251–79, 02 1984.
- [37] E. Salmon Powell, C. Carrico, E. Salyers, P. M. Westgate, and L. Sawaki, “The effect of transcutaneous spinal direct current stimulation on corticospinal excitability in chronic incomplete spinal cord injury,” *NeuroRehabilitation*, vol. 43, pp. 1–10, 07 2018.
- [38] A. Holtermann, C. Grnlund, J. Karlsson, and K. Roeleveld, “Motor unit synchronization during fatigue: Described with a novel semg method based on large motor unit samples,” *Journal of Electromyography and Kinesiology*, vol. 19, no. 2, pp. 232 – 241, 2009. [Online]. Available: <http://www.sciencedirect.com/science/article/pii/S1050641107001460>
- [39] I. A. Lazarevich, I. Prokin, and B. Gutkin, “Neural activity classification with machine learning models trained on interspike interval series data,” in *Cornell University arXiv*, 10 2018.
- [40] H. Amin and R. Fujii, “Spike train decoding scheme for a spiking neural network,” in *2004 IEEE International Joint Conference on Neural Networks (IEEE Cat. No.04CH37541)*, vol. 1, July 2004, pp. 477–482.
- [41] F. Kendall, E. McCreary, and P. Provance, *Muscles: Testing and Function with Posture and Pain*. Lippincott Williams & Wilkins, 2005. [Online]. Available: <https://books.google.nl/books?id=AgRkvidspkMC>
- [42] R. Drake, A. Vogl, A. Mitchell, R. Tibbitts, and P. Richardson, *Gray’s Atlas of Anatomy, Second Edition*. Churchill Livingstone, 01 2015.
- [43] W. Sharrard, “The segmental innervation of the lower limb muscles in man,” *Annals of the Royal College of Surgeons of England*, vol. 35, pp. 106–122, 08 1964.
- [44] D. G. Sayenko, D. A. Atkinson, T. C. Floyd, R. M. Gorodnichev, T. R. Moshonkina, S. J. Harkema, V. R. Edgerton, and Y. P. Gerasimenko, “Effects of paired transcutaneous electrical stimulation delivered at single and dual sites over lumbosacral spinal cord,” *Neuroscience Letters*, vol. 609, pp. 229 – 234, 2015. [Online]. Available: <http://www.sciencedirect.com/science/article/pii/S0304394015301683>
- [45] A. Kuck, “Trans-spinal direct current stimulation for the modulation of the lumbar spinal motor networks,” Ph.D. dissertation, University of Twente, Netherlands, 1 2018.